NASA TECHNICAL NOTE

NASA TN D-3064
C. 1

A DESCRIBING-FUNCTION ANALYSIS OF THE STABILITY OF A LAUNCH VEHICLE WITH NONLINEAR THRUST VECTORING

by Harold C. Lester

Langley Research Center
Langley Station, Hampton, Va.

NATIONAL AERONAUTICS AND SPACE ADMINISTRATION • WASHINGTON, D. C. • OCTOBER 1965

A DESCRIBING-FUNCTION ANALYSIS OF THE STABILITY OF A

LAUNCH VEHICLE WITH NONLINEAR THRUST VECTORING

By Harold C. Lester

Langley Research Center
Langley Station, Hampton, Va.

NATIONAL AERONAUTICS AND SPACE ADMINISTRATION

A DESCRIBING-FUNCTION ANALYSIS OF THE STABILITY OF A

LAUNCH VEHICLE WITH NONLINEAR THRUST VECTORING

By Harold C. Lester
Langley Research Center

SUMMARY

The stability characteristics of a representative launch vehicle utilizing a type of nonlinear thrust vectoring are investigated by the describing-function method. The nonlinearities in the system are associated with the control thrust forces which are produced by an auxiliary engine rotating through large gimbal angles with predetermined limits imposed on the amplitude of rotation. Limit amplitudes as large as ±90° are considered and a describing function is derived to approximate the nonlinearities introduced by the amplitude limits and the sine coupling of the control engine with the rigid-body launch-vehicle equations of motion. Stability bounds for the system are determined graphically by means of a gain-phase analysis for various combinations of the control system and excitation parameters. Selected stable limit cycles, predicted by the describing function analysis, are verified by using an analog computer simulation of the launch-vehicle configuration.

INTRODUCTION

The control and guidance of almost all present-day launch vehicles is achieved by thrust vectoring, that is, by swiveling the thrust chambers of all or some of the main booster engines to produce the desired stabilizing force components. Maximum thrust-vector-rotation angles required are usually less than ±10°. Although such a control method has been successful for past and current applications, new thrust-vector control techniques may be more suitable with future launch vehicles, particularly the large solid-propellant systems. A recently proposed method employs auxiliary control engines producing a much lower thrust than the main booster engines. In order to obtain lateral forces and pitching moments large enough to stabilize and control the vehicle, the control engines are rotated through much larger gimbal angles - as high as ±90°. Such a thrust vectoring scheme leads to nonlinear coupling of the control thrust with the vehicle equations of motion by virtue of the requirement for larger rotation angles. An additional nonlinearity is introduced by amplitude limits which are imposed on the control engine.

Linear stability methods - such as the Bode, Nyquist, and root-locus procedures - are not directly applicable for the study of nonlinear systems.

However, a linearization technique known as the describing-function method (ref. 1) can be used in certain cases to approximate the response characteristics of a nonlinear system in order to take advantage of the well-established methods of linear analysis. This method has been applied with success in analyzing servomechanisms involving such nonlinearities as off-on relays, saturation, dead band, coulomb friction, backlash, and hysteresis (refs. 1, 2, and 3). The method has also been used in analyzing off-on reaction control systems employed on the upper stages of vehicles for control and stability during the terminal phase of exit from the earth's sensible atmosphere and for attitude control in orbit (ref. 4). In addition, the describing function has been employed to study the nonlinearities present in a particular element within an open- or closed-loop system (ref. 5).

The present study examines the applicability of the describing-function method for investigating the stability of a launch vehicle having the aforesaid nonlinear thrust-vectoring characteristics. In the study, the gain-phase characteristics of the system nonlinearities are approximated by a describing function. The remaining portion of the control loop which is linear is represented by gain-phase plots, and the stability of a typical launch-vehicle configuration is determined graphically.

Motion in the pitch plane is considered and constant-coefficient differential equations, which describe the perturbations about a discrete point in an ascent trajectory, are used to represent the rigid-body dynamics of the launch vehicle. The control engine is positioned in accordance with command signals from an attitude and attitude-rate feedback sensor in the control loop. Parameters associated with a representative launch-vehicle configuration are evaluated at the maximum dynamic pressure condition and stability bounds are presented for various combinations of attitude and attitude-rate gains, control engine frequency and damping parameters, and excitation parameters. Selected stable limit cycles, predicted analytically, are verified by using an analog computer simulation of the system.

SYMBOLS

A nondimensional amplitude of unlimited sinusoidal response of control engine (eqs. (12))

a_0 control-system attitude gain

a_1 control-system attitude-rate gain, sec

B nondimensional amplitude associated with sinusoidal response of control engine with amplitude limits imposed (eq. (14))

D drag force, lb

g gravitational acceleration constant, in./sec^2

$G(s)$	transfer function for linear elements in open-loop system (eq. (24))
I	mass moment of inertia of launch vehicle about center of gravity, lb-sec^2-in.
k	index of summation
l	length of launch vehicle, in.
m	total mass of launch vehicle, lb-sec^2/in.
N	describing function (eq. (9))
$S(x)$	local cross-sectional area of revolution of launch vehicle about X-axis, in.^{2}
s	Laplace transform variable, 1/sec
T_b	booster thrust, lb
T_c	control thrust, lb
t	time, sec
V	velocity of launch vehicle, in./sec
X, Y	body axis coordinate system
x, y	coordinates along X and Y axes, in.
$\bar{x}$	coordinate locating center of gravity, in.
$\bar{y}$	normal perturbation variable, in.
β	control thrust (control engine) rotation angle, radian
β_c	control thrust command function, radian
β_l	limit amplitude, radian
β_o	amplitude of sinusoidal forcing function (eq. (7)), radian
δ	nondimensional control engine rotation angle, β/β_o
$\gamma = \sin \beta$	
γ_k	generalized coefficient associated with Fourier expansion of γ (eq. (8))
θ	attitude perturbation variable, radian

3

θ_e attitude error angle, radian

θ_f feedback signal, radian

θ_g phase angle associated with $G(s)$, radian

θ_p programed attitude, radian

μ attitude-rate gain parameter, a_0/a_1, 1/sec

ξ viscous damping ratio associated with control engine

ρ atmospheric density at altitude of interest, lb-sec^2/in^4

τ nondimensional time (eqs. (10))

τ_n particular value of nondimensional time τ for $n = 0, 1, 2, 3$, and 4 (see fig. (14))

τ' nondimensional time as measured from τ_2, that is, $\tau' = \tau - \tau_2$

σ nondimensional amplitude ratio, β_0/β_l

ϕ attitude associated with ideal ascent trajectory, radian

ϕ_n particular phase angle associated with sinusoidal response of control engine for $n = 0, 1,$ and 2, radian

ψ_k generalized phase angle associated with Fourier expansion of γ (eq. (8))

Ω nondimensional frequency ratio, ω/ω_n

Ω_d nondimensional damped frequency ratio, ω/ω_d

ω forcing function frequency (eq. (7)), radian/sec

ω_n undamped natural frequency of control engine, radian/sec

ω_d damped natural frequency of control engine, radian/sec

     A dot over a variable indicates a differentiation with respect to time t. A primed variable indicates a differentiation with respect to x. Bars over symbols denote vectors.

ANALYSIS

In this section the basic equations of motion are presented and discussed. A describing function is then calculated to account for the system nonlinearities. Finally, the transfer function of the closed-loop system is derived and the governing stability equations established.

System Equations

Coordinate system.- Generally, the stability of a launch vehicle is determined by analyzing the perturbation motion about a reference trajectory for discrete values of flight time. The situation is illustrated in figure 1 which shows the degrees of freedom employed in the present analysis: a normal translation of the center of gravity $\bar{y}$; a rigid-body rotation about the center of gravity θ; and a control thrust rotation angle β. It should be noted that the $\bar{y}$ and θ degrees of freedom represent small deviations from an equilibrium flight condition. The resulting perturbation equations have time-fixed coefficients and are linear in the variables $\bar{y}$ and θ.
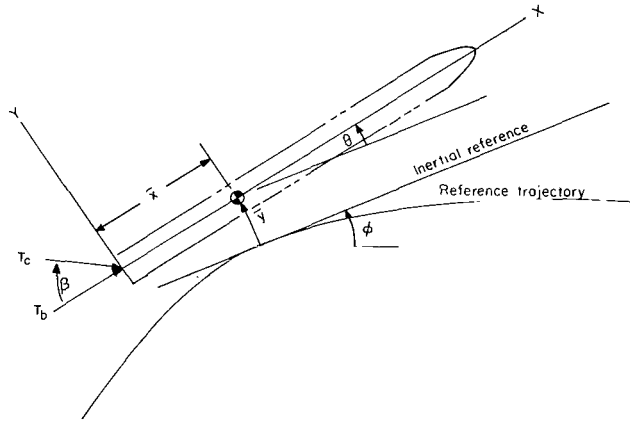
Equations of motion.- The equations of motion for the translation and pitch perturbations can be derived by the method of Lagrange (see, for example, ref. 6) and are summarized below:

Figure 1.- Coordinate system.

Normal perturbation equation:

$$\ddot{\bar{y}} = \left[\frac{\rho V}{m} \int_0^l S'(x)\,dx\right]\dot{\bar{y}} + \left[\frac{T_b - D}{m} - \frac{\rho V^2}{m} \int_0^l S'(x)\,dx\right]\theta$$

$$+ \left[\frac{\rho V}{m} \int_0^l (x - \bar{x}) S'(x)\,dx\right]\dot{\theta} - \left(\frac{T_c}{m}\right)\sin\beta \qquad (1)$$

Pitch perturbation equation:

$$\ddot{\theta} = \left[\frac{\rho V}{I} \int_0^{\mathit{l}} (x - \overline{x})\, S'(x)\, dx\right]\dot{\overline{y}} - \left[\frac{\rho V^2}{I} \int_0^{\mathit{l}} (x - \overline{x})\, S'(x)\, dx\right]\theta$$

$$+ \left[\frac{\rho V}{I} \int_0^{\mathit{l}} (x - \overline{x})^2\, S'(x)\, dx\right]\dot{\theta} + \left(\frac{T_c \overline{x}}{I}\right)\sin \beta \qquad (2)$$

In equations (1) and (2) the aerodynamic forces and moments have been developed by using an approximation of slender-body momentum theory (ref. 7). This theory gives the distributed aerodynamic lift (per unit length) as proportional to the derivative $S'(x)$, where $S(x)$ represents the local cross-sectional area of revolution of the launch vehicle about its longitudinal axis. One additional comment concerning the thrust forces is necessary. The total thrust component $T_{\overline{y}}$ acting in the $\overline{y}$ direction is given by the equation

$$T_{\overline{y}} = \left(T_b + T_c \cos \beta\right)\theta - T_c \sin \beta$$

where T_b and T_c are the booster and control thrust, respectively, and θ, it should be recalled, represents a small perturbation in pitch attitude. With the restriction that the ratio T_c/T_b be small relative to unity - for example, 0.1 or less - the following approximation

$$T_{\overline{y}} \approx T_b \theta - T_c \sin \beta$$

is assumed in deriving equation (1).

Control engine.- Launch vehicles are controlled by lateral-force components which for the configuration considered are obtained from an auxiliary control engine. This method differs somewhat from the conventional thrust vectoring method. The two methods may be compared with the aid of figure 2. As illustrated in part (a) of this figure, the conventional thrust vectoring method utilizes the thrust T_b of the main booster engines by rotating the thrust chamber through a small angular misalinement or gimbal angle β. Maximum gimbal angles are usually less than $\pm 10^{\circ}$. With the auxiliary control engine method, as shown in part (b) of figure 2, the main booster engines are fixed. Lateral thrust components are obtained in this case by rotating the control engine through gimbal angles which may be as large as $\pm 90^{\circ}$. With the conventional method, the lateral thrust components are proportional to the gimbal angle β (in radians) since rotation angles remain small. However, with the auxiliary engine method, the lateral thrust components are proportional to $\sin \beta$ and result in a nonlinear coupling with the rigid-body equations of motion. In addition, if the control engine is amplitude limited at some arbitrary level β_l, where $\beta_l \leqq \pm 90^{\circ}$, an additional nonlinear influence is possible.
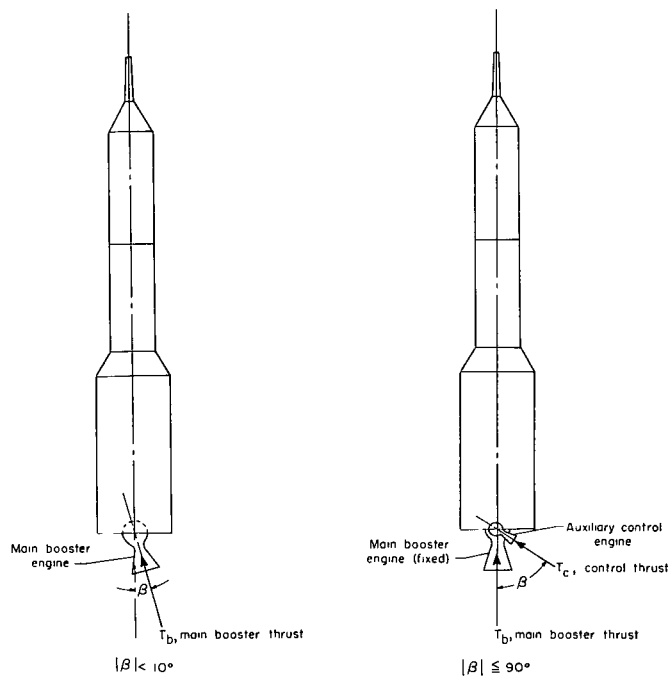
(a) Conventional method.   (b) Auxiliary control engine method.

Figure 2.- Methods of thrust vector control.

In the present analysis the control engine dynamics can be summarized by the following second-order differential equation:

$$\ddot{\beta} + 2\xi\omega_n\dot{\beta} + \omega_n^2\beta = \omega_n^2\beta_c \qquad (3)$$

subject to the boundary conditions or constraint equations

$$\left.\begin{array}{l} |\beta| \leqq \beta_l \\[2mm] \dot{\beta} = 0 \qquad \left(\beta = \pm\beta_l\right) \end{array}\right\} \qquad (4)$$

where β_l is an arbitrary limit amplitude and β_c is the command input to the control engine. (See appendix A.) It should be noted that for $\beta < \beta_l$, the response of the control engine is that of a damped linear second-order system. For $\beta = \beta_l$, however, the response is nonlinear as a result of the boundary conditions.

Control-system considerations.- The control-system block diagram is shown in figure 3. As indicated in the figure, an attitude and attitude-rate feedback sensor is assumed so that in the time domain the total feedback θ_f is given by the equation

7

$$\theta_f = \theta + \frac{1}{\mu} \dot{\theta} \tag{5}$$

where μ is an attitude-rate gain parameter which is defined as the ratio of the attitude gain a_0 to the attitude-rate gain a_1, that is,

$$\mu = \frac{a_0}{a_1} \tag{6}$$

In the expression for the total feedback signal (eq. (5)) the $\dot{\theta}$ component serves to introduce damping into the rigid-body control mode.
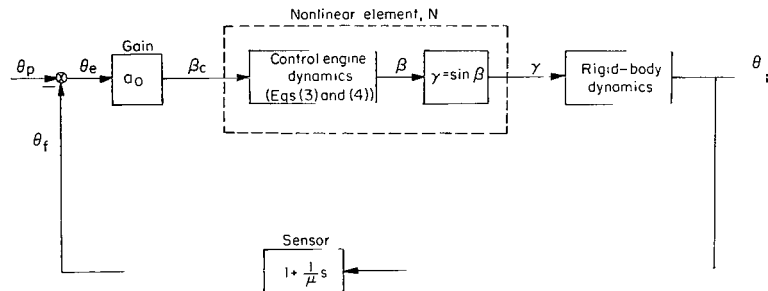

Figure 3.- System block diagram.

In addition, figure 3 illustrates the location of the system nonlinearities in relation to the closed-loop control-system structure. The nonlinearities are associated with the two forward path elements which are enclosed by the dashed line. The input to the total equivalent nonlinear element N is β_c, the control engine command signal. As indicated by equations (3) and (4), the output response β of the control engine may be either linear or nonlinear depending on whether the control engine limits $\left(\beta = \pm\beta_l\right)$. Finally, the $\sin\beta$ coupling of the control thrust with the translation and pitch degrees of freedom is indicated in figure 3 by the output signal γ of the nonlinear element. In the ensuing section a describing function N is derived to approximate the frequency-response characteristics of the system nonlinearities.

Describing-Function Procedure

General procedure.- The Nyquist, Bode, and root-locus procedures which form the basis of feedback system analysis are limited in applicability to linear systems. Methods available for the analysis of nonlinear systems are not nearly as plentiful and as general in application as those developed for linear systems. The phase-plane method, for example, requires that a system be representable by a single second-order differential equation and only predicts the transient response from a given initial state.

The difficulties encountered in nonlinear analysis are related to the exceedingly complex behavior of nonlinear systems as compared with linear systems. For example, the response of a linear system is linearly dependent

on the amplitude of applied excitation; doubling the input amplitude merely increases the amplitude of the output by the same multiple. With nonlinear systems, the output can be significantly dependent on the level or amplitude of excitation. Furthermore, if a linear system is excited by a sinusoidal forcing function, the output will be a sinusoid of different amplitude and phase but having the same frequency. The output of nonlinear systems forced in a similar manner may contain harmonics of the excitation frequency. One peculiarity common to nonlinear systems which will be of interest in the present analysis will be constant-amplitude oscillations known as limit cycles.

The describing-function technique is a linearization method based on the assumption that the input to the nonlinear element in a system is a sinusoid (refs. 1, 2, and 3). Graphically, this method is illustrated in figure 3 which shows the block diagram of the system under consideration. The nonlinear element shown here represents the totality of all nonlinearities contained within the system. The input to the nonlinear element is assumed as

$$\beta_c = \beta_0 \sin \omega t \tag{7}$$

that is, a sinusoid of amplitude β_0 and frequency ω. The output $\gamma(t)$ is then expressed in the form of a Fourier sine series

$$\gamma(t) = \underbrace{\gamma_1 \sin\left(\omega t + \psi_1\right)}_{\text{Fundamental}} + \underbrace{\sum_{k=3,5,\ldots} \gamma_k \sin\left(k\omega t + \psi_k\right)}_{\text{Higher order terms}} \tag{8}$$

where the coefficients γ_k (for $k = 1,3,5,\ldots$) are functions of both β_0 and ω. It should be noted that the even coefficients ($k = 2,4,6,\ldots$) are identically zero since these terms evolve from an integration over the half period ($0 \leqq \omega t \leqq \pi$) of the product of an even and odd function. The key assumption on which the validity of the describing function depends is that only the fundamental component of the output is fed back and contributes significantly to the input of the nonlinear element. (See ref. 2.) This assumption is permissible on the grounds that the passive elements in the loop act as low-pass filters and attenuate the higher harmonics to a greater extent than the fundamental.

The describing function N is defined as the ratio of the coefficient of the fundamental to the amplitude of the input (refs. 1, 2, and 3):

$$N\left(\beta_0, \omega\right) \equiv \frac{\gamma_1\left(\beta_0, \omega\right)}{\beta_0}, \quad \underline{/\psi_1\left(\beta_0, \omega\right)} \tag{9}$$

and can be interpreted as a linear element in the control loop which has an amplitude β_0 as well as frequency-dependent ω gain and phase. When γ_1 is independent of frequency, the describing function is said to represent a simple nonlinearity. In such cases, the phase angle of N is zero and only the gain of the system is affected. If the describing function is both amplitude and

frequency dependent, it is said to define a complex nonlinearity. The describing-function method enables the analyst to retain use of the linear techniques of analysis by extending these methods to compensate for the variable gain and phase of the nonlinear element.

Derivation of the describing function.- Describing-function analysis of the control engine requires that the forcing input to the control engine be assumed as a sinusoid. Thus, it is necessary to determine a solution to equations (3) and (4) with β_c given by equation (7). By using the following non-dimensional parameters

$$\left.\begin{array}{c} \tau = \left(\dfrac{\omega}{2\pi}\right)t \\[2ex] \Omega = \dfrac{\omega}{\omega_n} \\[2ex] \Omega_d = \dfrac{\omega}{\omega_d} = \dfrac{\Omega}{\sqrt{1 - \xi^2}} \\[2ex] \sigma = \dfrac{\beta_o}{\beta_l} \\[2ex] \delta = \dfrac{\beta}{\beta_o} \end{array}\right\} \tag{10}$$

the sinusoidal response of the control engine is derived in appendix A and the solutions for both the linear and nonlinear response modes may be summarized as follows:

Linear-response equations $\left(A \leqq \dfrac{1}{\sigma}\right)$:

$$\delta(\tau) = A \sin\left(2\pi\tau - \phi_2\right) \tag{11}$$

where

$$\left.\begin{array}{c} A = \dfrac{1}{\sqrt{4\xi^2\Omega^2 + \left(1 - \Omega^2\right)^2}} \\[3ex] \phi_2 = \tan^{-1}\left(\dfrac{2\xi\Omega}{1 - \Omega^2}\right) \end{array}\right\} \tag{12}$$

Nonlinear-response equations $\left(A > \dfrac{1}{\sigma}\right)$:

$$\delta(\tau) = -A \sin\left(2\pi\tau + \pi - \phi_2\right) - B\left\{\exp\left[-\frac{2\pi\xi}{\Omega}\left(\tau - \tau_2 + \frac{1}{2}\right)\right]\right\} \sin\left[\frac{2\pi}{\Omega_d}\left(\tau - \tau_2 + \frac{1}{2}\right) + \phi_0\right]$$

$$\left(0 \leqq \tau \leqq \tau_1\right) \qquad (13a)$$

$$\delta(\tau) = \frac{1}{\sigma} \qquad \left(\tau_1 \leqq \tau \leqq \tau_2\right) \qquad (13b)$$

$$\delta(\tau) = A \sin\left(2\pi\tau - \phi_2\right) + B\left\{\exp\left[-\frac{2\pi\xi}{\Omega}\left(\tau - \tau_2\right)\right]\right\} \sin\left[\frac{2\pi}{\Omega_d}\left(\tau - \tau_2\right) + \phi_0\right]$$

$$\left(\tau_2 \leqq \tau \leqq \tau_3\right) \qquad (13c)$$

$$\delta(\tau) = -\frac{1}{\sigma} \qquad \left(\tau_3 \leqq \tau \leqq \tau_4\right) \qquad (13d)$$

$$\delta(\tau) = -A \sin\left(2\pi\tau - \pi - \phi_2\right) - B\left\{\exp\left[-\frac{2\pi\xi}{\Omega}\left(\tau - \tau_4\right)\right]\right\} \sin\left[\frac{2\pi}{\Omega_d}\left(\tau - \tau_4\right) + \phi_0\right]$$

$$\left(\tau_4 \leqq \tau \leqq 1.0\right) \qquad (13e)$$

where

$$B = \frac{\frac{1}{\sigma} - A \sin \phi_1}{\sin \phi_0} \qquad (14a)$$

$$\Omega_d = \frac{\Omega}{\sqrt{1 - \xi^2}} \qquad (14b)$$

$$\phi_0 = \tan^{-1}\left[\frac{\frac{1}{\sigma} - A \sin \phi_1}{\xi \frac{\Omega_d}{\Omega}\left(\frac{1}{\sigma} - A \sin \phi_1\right) - \Omega_d A \cos \phi_1}\right] \qquad (14c)$$

$$\phi_1 = 2\pi\tau_2 - \phi_2 \qquad (14d)$$

$$\tau_0 = \frac{1}{2\pi} \sin^{-1}\left(\frac{1}{\sigma}\right) \qquad (\sigma > 1.0) \qquad (14e)$$

$$\tau_3 = \tau_1 + \frac{1}{2} \qquad (14f)$$

$$\tau_4 = \tau_2 + \frac{1}{2} \qquad (14g)$$

and where τ_3 can be found by solving the equation

$$A \sin\left(2\pi\tau_3 - \phi_2\right) + B\left\{\exp\left[-\frac{2\pi\xi}{\Omega}(\tau_3 - \tau_2)\right]\right\} \sin\left[\frac{2\pi}{\Omega_d}(\tau_3 - \tau_2) + \phi_0\right] + \frac{1}{\sigma} = 0 \qquad (15a)$$

subject to the conditions:

$$\tau_2 = \frac{1}{2} - \tau_0 \qquad (\sigma > 1.0) \qquad (15b)$$

$$\tau_3 - \tau_2 = \frac{1}{2} \qquad (\sigma \leqq 1.0) \qquad (15c)$$

In order to verify the solution as given by equations (10) to (15), an analog computer solution of equations (3), (4), and (7) was effected. The results, for several input conditions, are presented in figure 4. Part (a) of figure 4 illustrates the response obtained with a damping ratio of $\xi = 0.4$ when the system is excited near resonance $\frac{\omega}{\omega_n} = 1.2$ and forced with an amplitude which is twice the limit amplitude $\frac{\beta_0}{\beta_l} = 2$. In part (b) of figure 4, the damping and frequency ratios have been decreased to $\xi = 0.2$ and $\frac{\omega}{\omega_n} = 0.6$ and the system excited by a level of excitation equal to the limit amplitude $\frac{\beta_0}{\beta_l} = 1$. In part (c) of figure 4 the resonant response of the system is illustrated for a damping ratio of $\xi = 0.2$ and a forcing amplitude equal to one-half the limit value $\frac{\beta_0}{\beta_l} = 0.5$. Since, in this latter case, the system is excited at its resonant frequency, the system experiences limiting and the resulting response is cusped; that is, the control engine does not remain on the limit for a finite time.

The preceding paragraphs have discussed the steady-state response of the control engine when excited by a sinusoidal forcing function. The describing function for the total nonlinear element (see fig. 3) must also account for the nonlinear coupling of the control engine with the translation and pitch degrees of freedom. Thus, the output from the total nonlinear element is given by the equation

12

$$\gamma = \sin \beta \tag{16}$$

where β and δ (eqs. (10)) are related by the following equation:

$$\beta = \left(\beta_l \sigma\right)\delta \tag{17}$$

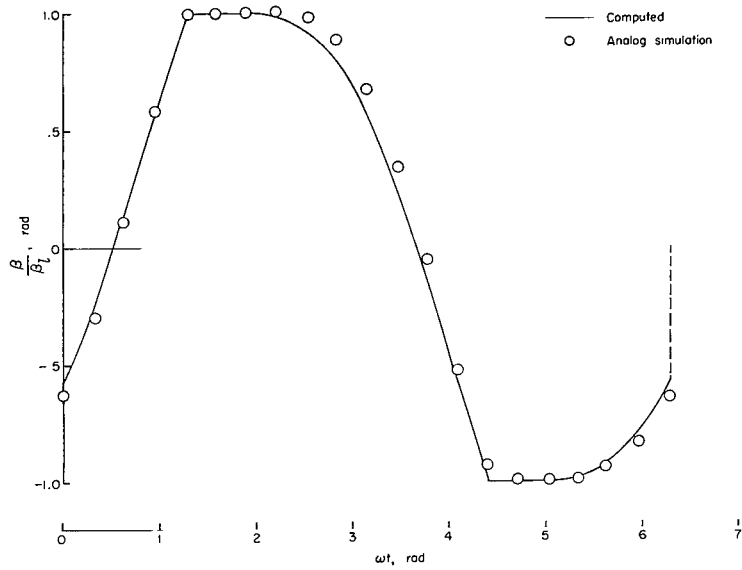The equations for δ, β, and γ (eqs. (10) to (17)) were programed on a digital computer and were evaluated for various combinations of the frequency ratio $\Omega = \dfrac{\omega}{\omega_n}$, amplitude ratio $\sigma = \dfrac{\beta_o}{\beta_l}$, and for two values of damping $\xi = 0.4$ and $\xi = 0.7$. By using a digital integration routine, the amplitude γ_1 and phase angle ψ_1 of the fundamental were computed and, as stated previously in equation (9), the describing function for the system was determined.

Results are presented in figure 5 which shows the variation of the amplitude of the inverse describing function $1/N$ with its phase angle $180^\circ - \psi_1$. The inverse form is used for convenience, as will be apparent in a later section. The results of figure 5 are generalized in terms of the nondimensional parameters σ and Ω (see eqs. (10)) representing an amplitude and frequency ratio, respectively. As is apparent from the figure, if the natural frequency ω_n of the control engine is specified and a particular limit amplitude value β_l chosen, the describing function or rather its inverse can be considered a function of the excitation amplitude and frequency, that is, a function of β_o and ω. It should be noted that the describing function possesses both an amplitude ratio and a phase angle and therefore alters both the gain and phase of the system. In addition, as a result of the amplitude limits, the response of the fundamental possesses a jump region in the gain-phase plane.
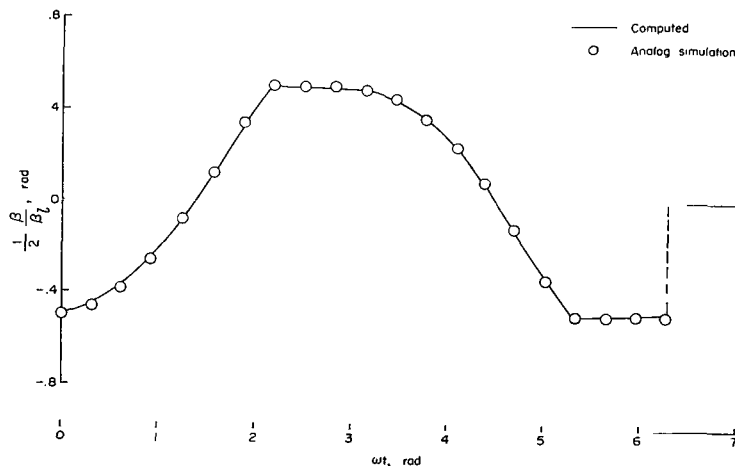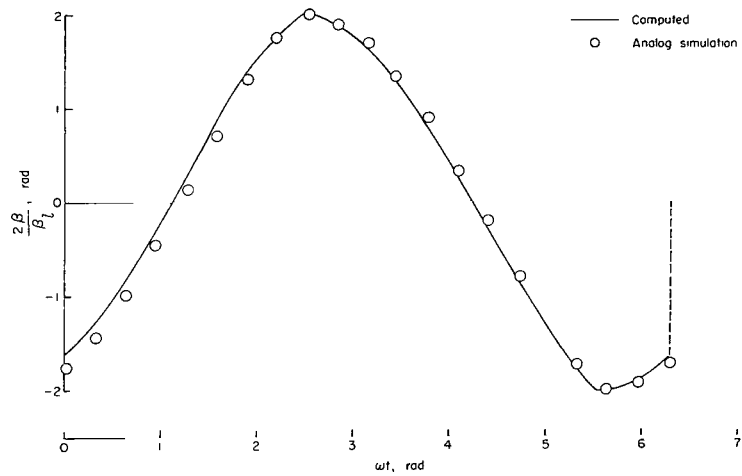

(a) $\dfrac{\beta_0}{\beta_l} = 2;\ \dfrac{\omega}{\omega_n} = 1.2;\ $ and $\ \xi = 0.4.$

Figure 4.- Response to sinusoidal input of control engine with an amplitude limit.

Computed

○ Analog simulation

$\frac{\beta}{\beta_l}$, rad

ωt, rad

(b) $\frac{\beta_0}{\beta_l} = 1$; $\frac{\omega}{\omega_n} = 0.6$; and $\xi = 0.2$.

Computed

○ Analog simulation

$\frac{2\beta}{\beta_l}$, rad

ωt, rad

(c) $\frac{\beta_0}{\beta_l} = 0.5$; $\frac{\omega}{\omega_n} = 1.0$; and $\xi = 0.2$.

Figure 4.- Concluded.

14

(a) $\xi = 0.7$.

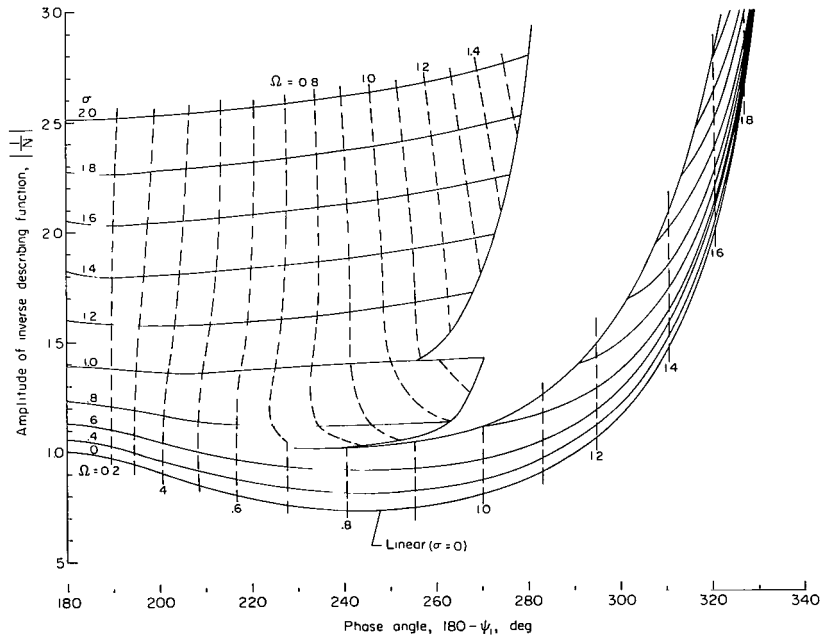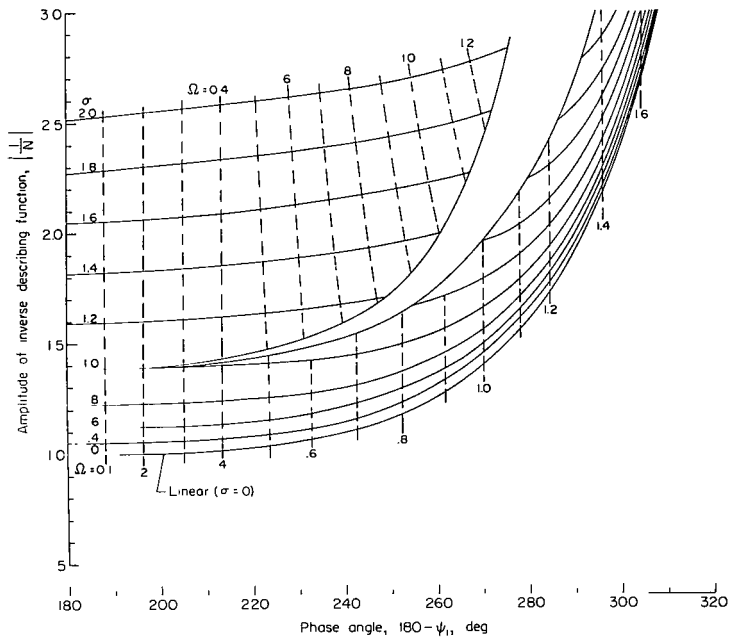
(b) $\xi = 0.4$.

Figure 5.- Inverse describing functions.

Derivation of System Transfer Function

In a purely linear control system, the transfer functions of the individual elements may be cascaded in any order to produce the net gain and phase shift between two points in the control loop. Similarly, interpreting the describing function as an equivalent linear element with an amplitude- and frequency-dependent gain and phase leads readily to the formulation of the open-loop transfer function of the system analyzed herein.

From figure 3 the transfer function for the forward loop may be written as follows:

$$\frac{\theta(s)}{\theta_e(s)} = \frac{\gamma(s)}{\theta_e(s)} \frac{\theta(s)}{\gamma(s)} \tag{18}$$

By substituting $a_0 N$ for $\gamma(s)/\theta_e(s)$ and letting N the describing function, represent the combined gain-phase characteristics of the nonlinear element, the preceding equation for $\theta(s)/\theta_e(s)$ becomes

$$\frac{\theta(s)}{\theta_e(s)} = a_0 N \frac{\theta(s)}{\gamma(s)} \tag{19}$$

The transfer function $\theta(s)/\gamma(s)$ can be obtained from the rigid-body equations (eqs. (1) and (2)) by substituting the results of equation (16). If the Laplace transform is taken with respect to the variable t, all initial conditions assumed to be identically zero, and the terms collected, equations (1) and (2) can be arranged into the following matrix form:

$$\begin{bmatrix} a_{11} & a_{12} \\ a_{21} & a_{22} \end{bmatrix} \begin{Bmatrix} \overline{y}(s) \\ \theta(s) \end{Bmatrix} = \gamma(s) \begin{Bmatrix} a_{13} \\ a_{23} \end{Bmatrix} \tag{20}$$

where the coefficients a_{ij} (where i and j are 1, 2, . . .) may be determined by carrying out the transformation and identifying like terms in equations (1), (2), and (20). If the determinants $A(s)$ and $C(s)$ are introduced and defined as

$$A(s) = \begin{vmatrix} a_{11} & a_{13} \\ a_{21} & a_{23} \end{vmatrix}$$

$$C(s) = \begin{vmatrix} a_{11} & a_{12} \\ a_{21} & a_{22} \end{vmatrix}$$

The required transfer function may be written as follows:

$$\frac{\theta(s)}{\gamma(s)} = \frac{A(s)}{C(s)} \tag{21}$$

The transfer function for the feedback path is given by the following equation:

$$\frac{\theta_f(s)}{\theta(s)} = \frac{1}{\mu}(s + \mu) \tag{22}$$

and hence the open-loop transfer function of the system is simply

$$\frac{\theta_f(s)}{\theta_e(s)} = \frac{\theta(s)}{\theta_e(s)} \frac{\theta_f(s)}{\theta(s)}$$

which becomes on substitution of the results of equations (19) and (22)

$$\frac{\theta_f(s)}{\theta_e(s)} = \frac{a_0 N}{\mu} \frac{A(s)}{C(s)}(s + \mu) \tag{23}$$

By letting

$$G(s) = \frac{a_0}{\mu} \frac{A(s)}{C(s)}(s + \mu) \tag{24}$$

and substituting $s = j\omega$, where $j = \sqrt{-1}$, the open-loop transfer function may be written in a more usable form as follows:

$$\frac{\theta_f(\omega)}{\theta_e(\omega)} = N(\beta_0, \omega)G(\omega) \tag{25}$$

It should be noted that $G(s)$ represents the transfer function of the linear elements in the open-loop system. (See fig. 3.) In a similar manner, N represents the equivalent transfer function for all the nonlinearities in the open loop.

Method for Determining System Stability Graphically

By using equations (19) and (25), the closed-loop transfer function $\theta(s)/\theta_p(s)$ for the system may be formulated as

$$\frac{\theta(s)}{\theta_p(s)} = \frac{\theta(s)/\theta_e(s)}{1 + N\,G(s)} \tag{26}$$

17

where the numerator is the transfer function of the elements in the forward loop. The characteristic stability equation for the system is obtained by equating the denominator of equation (26) to zero; that is,
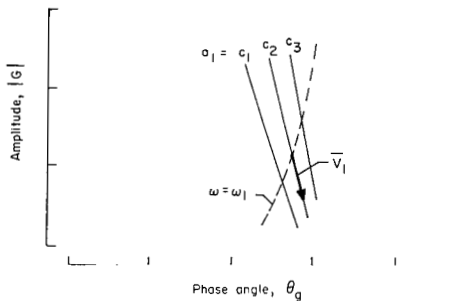
$$1 + N\,G(s) = 0 \tag{27}$$

Solutions of this equation represent conditions of marginal (neutral) stability. Rearranging equation (27) and expressing the results in a polar form produces the following equivalent equations which may be solved graphically:

$$\left.\begin{aligned} \left|G(\omega)\right| &= \frac{1}{\left|N(\beta_o,\omega)\right|} \\ \theta_g(\omega) &= 180^\circ - \psi_1(\beta_o,\omega) \end{aligned}\right\} \tag{28}$$

where the substitution $s = j\omega$ has been made.

(a) Typical gain-phase plot for $G(\omega)$.

(b) Inverse describing function $1/N$.

Figure 6.- Illustration of graphical solution in gain-phase plane.

In order to effect a graphical solution of equations (28), the amplitude $|G|$ is plotted against the phase angle θ_g with the frequency ω as a parameter. A typical plot is illustrated in part (a) of figure 6 for several values C_1, C_2, and C_3 of the attitude-rate gain a_1. The vector $\overline{V}_1$ is drawn tangent to the $a_1 = C_2$ curve and is directed in the sense of increasing frequency. An inverse describing-function plot is then dimensionalized by selecting a value for the natural frequency ω_n of the control engine and by using equations (10) to convert the constant Ω curves to constant ω curves. A typical inverse describing-function plot is shown in part (b) of figure 6 for several values of the amplitude ratio σ_1, σ_2, ... The vector $\overline{V}_2$ is drawn tangent to the $\omega = \omega_1$ curve and is directed in the sense of increasing amplitude ratio σ (assuming $\sigma_4 > \sigma_3 > \sigma_2 > \sigma_1$) where σ is defined by equations (10).

Once the inverse describing function has been dimensionalized, equations (28) may be solved graphically (ref. 3) by superimposing parts (a) and (b) of figure 6. Solutions are represented by those intersections which occur at a common frequency ω. The procedure is illustrated in part (c) of figure 6. An intersection, that is, a solution, is indicated for a frequency of $\omega = \omega_1$. The amplitude ratio σ

for the solution is between $\sigma = \sigma_2$ and
$\sigma = \sigma_3$ and the attitude-rate gain is
$a_1 = C_2$.

Solutions of equations (28) determine
conditions of marginal stability known as
limit cycles. If a limit cycle is stable,
the system will return or converge, after a
slight disturbance, to the marginal stability
condition. If the system diverges, the limit
cycle is unstable.

In general, a rigorous definition of sta-
bility, that is, whether a solution of equa-
tions (28) represents a stable or unstable
limit cycle, is difficult to formulate.
Instead, an argument is presented based on an
intuitive extension of the definition of sta-
bility for linear systems. The argument pro-
ceeds as follows: Let $\widetilde{G}(\omega)$ represent the
open-loop transfer function of a linear sys-
tem. By using the Nyquist stability method,
$\widetilde{G}(\omega)$ is plotted in the complex plane (for
$0 \leqq j\omega < j\infty$) as shown, for example, in
part (a) of figure 7. A circle of unit
radius is then constructed about the origin
and the intersection of this circle with the
negative real axis defines the critical point
$-1 + j0$. Within the framework of the abbre-
viated Nyquist method (if it is assumed that
the open-loop transfer function $\widetilde{G}(\omega)$ is
stable), the relative stability of the closed-
loop system may be determined by the amount
of phase margin ψ present when $G(\omega) = 1$
or rather, when $G(\omega)$ intersects the unit
circle. For example, at point A in part (a)
of figure 7 the phase margin ψ_A is positive
(by definition) and the system is stable,
since the Nyquist plot of $G(\omega)$ does not
encircle the critical point $-1 + j0$. If
$G(\omega)$ intersected the unit circle at point B
where the phase margin ψ_B is negative, the
closed-loop system would be unstable. In
summary the system is stable if the phase
margin is positive and unstable if the phase
margin is negative. The condition of mar-
ginal or neutral stability occurs for zero
phase margin.

The preceding ideas may be extended
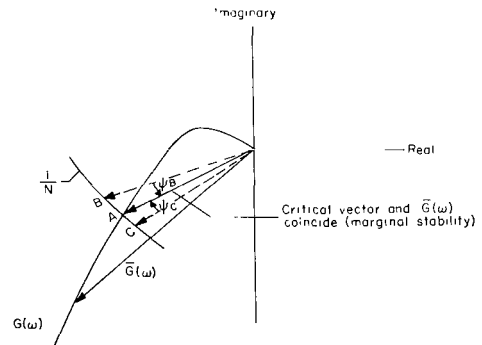intuitively to a nonlinear system with an
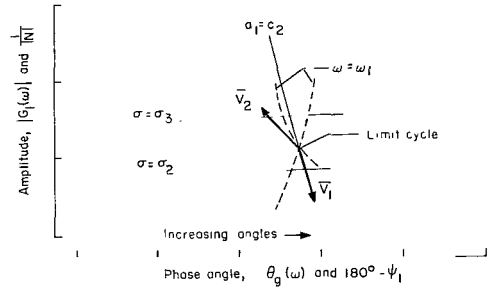
(c) Typical graphical solution resulting when the
gain-phase plot and the inverse describing
function are superimposed.

Figure 6.- Concluded.
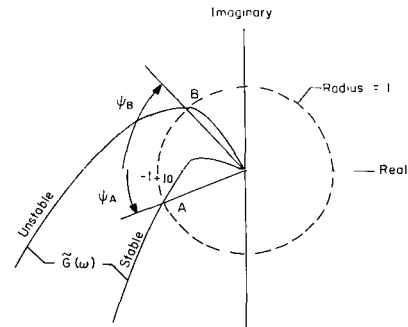
(a) Typical Nyquist plot for a linear system.

(b) Illustration of the describing function
method using a Nyquist plot.

Figure 7.- Comparison of the Nyquist stability
method as applied to linear and nonlinear
systems.

amplitude- and frequency-dependent describing function. In this case, the critical point is located in the complex plane by the critical vector

$$\frac{1}{\left|N\left(\beta_o,\omega\right)\right|}, \quad \underline{/180^o - \psi_1\left(\beta_o,\omega\right)}$$

where it is apparent that both the magnitude and direction of this vector vary with β_o and ω. As illustrated in part (b) of figure 7, a solution is shown at point A. Since the solution represents a point of marginal stability (zero phase margin) the critical vector and the $\overline{G}(\omega)$ vector coincide ($\overline{G}$ is the vector which traces out the $G(\omega)$ locus).

Suppose that position A is a solution and that the describing function $N\left(\beta_o,\omega\right)$ is such that a minute increase in amplitude $\left(\beta_o\right)$ moves the critical vector to position B. Based on the ideas presented previously for linear systems, one is tempted to interpret the angle ψ_B as a small increment of positive (stable) phase margin and to conclude that the critical vector has shifted its direction so that the closed-loop system is stable for increasing amplitudes. If the system is stable, the solution will eventually return or converge back to position A and, on this basis, the solution may be classified as a stable limit cycle. Conversely, with decreasing amplitudes, the critical vector will shift to position C where the phase margin ψ_C is negative and the system is unstable. As a result, the system will diverge and with increasing amplitudes the solution at position A will again be reached. For a solution to be classified as an unstable limit cycle, it appears that increasing (decreasing) amplitudes must produce negative (positive) phase margins.

Although the preceding argument lacks a rigorous proof, it appears to parallel similar types of reasoning given in the literature (refs. 1, 2, and 3) and is probably applicable to a wide variety of situations. In any case, as an analog computer simulation confirmed, this type of argument did prove to be adequate in classifying the stability boundaries for the system and nonlinearities discussed in this paper.

If reference is made to part (c) of figure 6 and this type of argument is used, the solution (intersection) may be classified as either a stable or unstable limit cycle. By assuming that $\sigma_3 > \sigma_2$, it is apparent that a small increase in the amplitude ratio σ moves the critical vector in the direction of the vector $\overline{V}_2$ and results in a small increment of positive phase margin since θ_g is now slightly greater than the phase angle $180^o - \psi_1$. The solution is thus a stable limit cycle.

To conclude this section, the following rule (from ref. 3), which may be helpful in classifying limit cycles, is given. The rule is paraphrased here to fit the specific situation illustrated in part (c) of figure 6. Consider an observer on a curve of constant attitude-rate gain - in this case the $a_1 = C_2$ curve - facing in the direction of increasing frequency, that is, in the direction indicated by vector $\overline{V}_1$. (The vector $\overline{V}_1$, it should be recalled, is

tangent to the $a_1 = C_1$ curve.) Now consider the vector $\overline{V}_2$ which originates on the inverse describing-function plot and is tangent to a line of constant frequency - in this case the $\omega = \omega_1$ curve. (It should be recalled that $\overline{V}_2$ is directed in the sense of increasing amplitude σ.) The rule may be stated as follows: If, to an observer looking along the vector $\overline{V}_1$ the vector $\overline{V}_2$ crosses from left to right, the solution (intersection) represents a stable limit cycle; if it crosses from right to left, the limit cycle is unstable.

DISCUSSION OF RESULTS

In this section the describing-function analysis outlined in the preceding section is employed to determine the stability characteristic of a hypothetical launch vehicle for the maximum dynamic pressure condition of a nominal ascent trajectory. Stability bounds are established for small control engine rotation angles, when the response of the system is essentially linear, by the root-locus method. Then by using the inverse describing function computed previously and representing the linear portion of the open-loop transfer function by gain-phase plots, stability bounds for the nonlinear mode are determined graphically. Finally, an analog computer simulation of the launch-vehicle system is used to verify the describing-function results.

Physical System

The hypothetical launch vehicle analyzed in this study consists of a multi-stage configuration with an overall length to first-stage diameter ratio of about 8.3. The thrust-weight ratio is about 1.25 and the control thrust level was selected as 10 percent of the total booster thrust, that is, $\frac{T_c}{T_b} = 0.1$. The control engine is allowed to rotate through gimbal angles as large as $\pm 90^\circ$, but may be arbitrarily limited at any amplitude up to and including this level. Values for the coefficients required in equations (1) and (2) are given in appendix B.

Linear Stability

For small amplitudes of oscillation the response of the control engine is linear and is governed solely by equation (3). In addition, the coupling of the control thrust with equations (1) and (2) may be satisfactorily approximated by replacing $\sin \beta$ with β (in radians). The transfer function for the control engine is therefore given by the equation

$$\frac{\beta(s)}{\beta_c(s)} = \frac{\omega_n^2}{s^2 + 2\xi\omega_n s + \omega_n^2}$$

which may be cascaded with the remaining elements of the control loop (eq. (24)) to produce the open-loop transfer function of the linear system

$$\left.\frac{\theta_f(s)}{\theta_e(s)}\right]_{Linear} = \frac{a_0 \omega_n^2}{\mu}\left[\frac{A(s)\ (s+\mu)}{C(s)\ \left(s^2 + 2\xi\omega_n s + \omega_n^2\right)}\right]$$

The closed-loop linear stability of the launch-vehicle configuration was determined by the root-locus method (ref. 2). The locus of roots is determined by equating the denominator of the closed-loop transfer function to zero, that is,

$$\left.\frac{\theta_f(s)}{\theta_e(s)}\right]_{Linear} + 1 = 0$$

and plotting the roots as a function of the open-loop gain in the complex plane.

By using the root-locus method, it is possible to establish regions of stability in terms of the control parameters a_0 and μ. These results are presented in figure 8 for several engine frequencies ω_n. Part (a) of figure 8 presents the stability boundaries for an engine damping of $\xi = 0.7$. With an attitude gain of $a_0 = 10$ and an engine frequency of $\omega_n = 2$, the vehicle is stable for $0.35 \leqq \mu \leqq 1.2$. If the engine frequency is increased to $\omega_n = 4$, the limits on μ become about $0.13 \leqq \mu \leqq 2.7$. For a given engine frequency, for example, $\omega_n = 3$, the attitude gain may only be increased to about $a_0 = 34$ at which the vehicle is unstable for any choice of the attitude-rate gain parameter μ. Hence, attitude gains greater than $a_0 = 34$ require engine frequencies greater than $\omega_n = 3.0$. The results presented in part (b) of figure 8 for $\xi = 0.4$ may be interpreted in a similar manner. The choice of μ for a
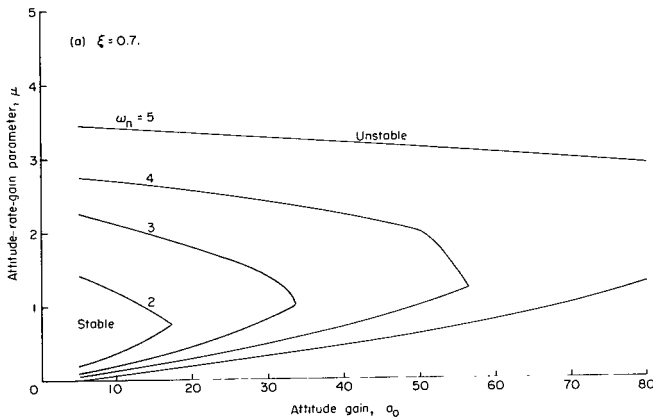
(a) $\xi = 0.7$.
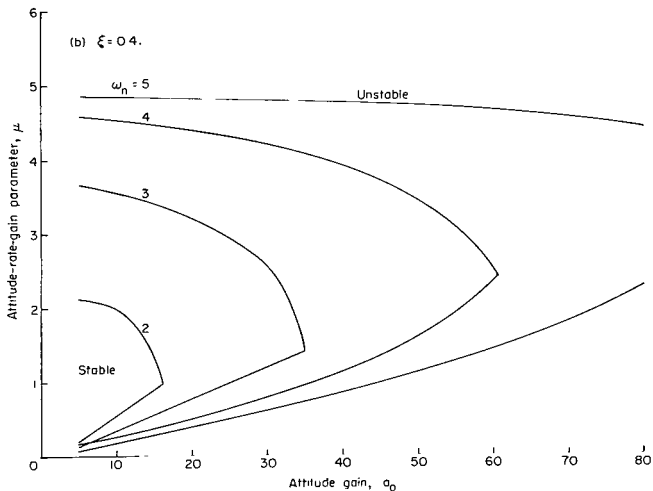
(b) $\xi = 0.4$.

Figure 8.- Linear stability boundaries.

particular a_0 determines the damping of the pitch mode, the smaller values of μ producing better damped responses. It should be recalled that the attitude rate gain a_1 is inversely proportional to μ as indicated by equation (6).

Nonlinear Stability

In general, disturbances such as winds and maneuver requirements will necessitate larger gimbal angles. It is therefore necessary to ascertain the stability characteristics of the system for the nonlinear mode when larger rotation angles are required. Since the describing function, as illustrated in figure 5, possesses both a gain and a phase angle, the root-locus method is too cumbersome for efficient use. Instead, a graphical solution is effected in the gain-phase plane as has been previously outlined in the "Analysis" section. The following numerical example is presented as being illustrative of the graphical method for determining stability bounds of the nonlinear mode.

A typical variation of gain with phase for $G(\omega)$ is presented in figure 9 for an attitude gain of $a_0 = 20$. By using the results of figures 5 and 9, a solution of equations (28) can be briefly demonstrated (see discussion following eqs. (28)) by considering, for example, the following choice of parameters:

$$\omega_n = 2$$

$$\xi = 0.4$$

$$a_0 = 20$$

Since an engine frequency has been specified, the inverse describing-function plot illustrated in part (b) of figure 5 may be dimensionalized in terms of the frequency ω by using equations (10). Hence, constant Ω curves are converted to constant ω curves. A graphical solution can now be obtained by superimposing part (b) of figure 5 on figure 9 and determining the intersections that occur at a common frequency.

One such intersection is illustrated in part (a) of figure 10 for an attitude-rate gain of about $a_1 = 35$. The corresponding frequency is $\omega = 2$
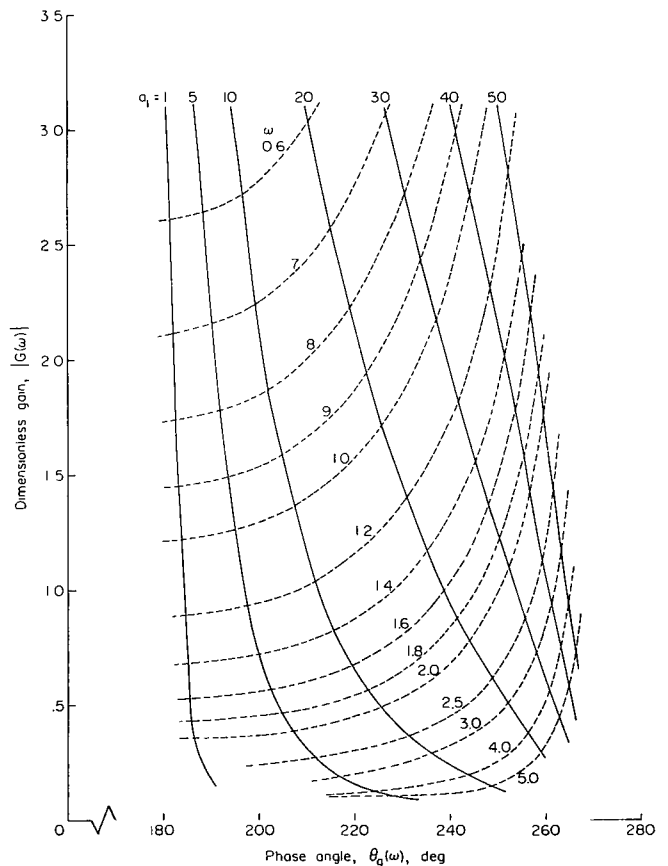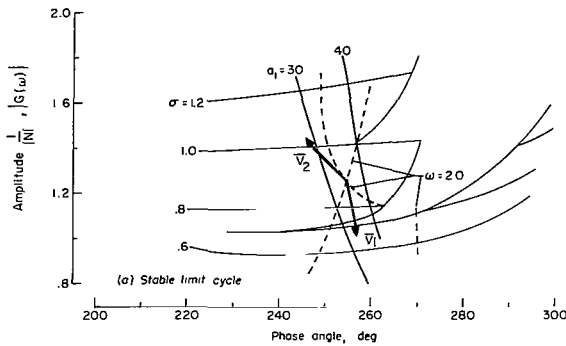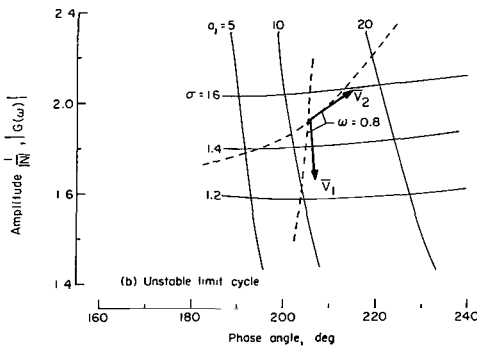

Figure 9.- Typical gain-phase plot of $G(\omega)$ for $a_0 = 20$.

(a) Stable limit cycle.

(b) Unstable limit cycle.

Figure 10.- Typical limit cycles illustrating the graphical solution for $a_0 = 20$, $\omega_n = 2$, and $\xi = 0.4$.

and the amplitude ratio is about $\sigma = 0.9$. The nature of the intersection may be determined by applying the rule given previously. Recall first that the vector $\overline{V}_1$ originates on the $G(\omega)$ plot and is constructed tangent to the $a_1 = 35$ curve and points in the direction of increasing frequency ω, whereas the vector $\overline{V}_2$ originates on the $1/N$ plot and is drawn tangent to the $\omega = 2$ curve and points in the direction of increasing amplitude σ. Since, to an observer looking along the $\overline{V}_1$ vector, the vector $\overline{V}_2$ crosses from left to right, the intersection (solution) is a stable limit cycle. Therefore, when the system is operating with this combination of parameters, that is, $a_0 = 20$, $a_1 = 35$, $\omega_n = 2$, and $\xi = 0.4$, a steady-state oscillation of amplitude ratio $\dfrac{\beta_0}{\beta_l} = 0.9$ and frequency $\omega = 2$ radians per second will develop and will persist indefinitely. Note should be made of the fact that the amplitude β_0 of the input signal β_c to the nonlinear element (fig. 3) can only be determined once a finite value has been assigned to the limit amplitude β_l; for example, if the control engine is limited at $\beta_l = \pm 45^\circ$, then the limit cycle is such that the input amplitude is about $\beta_0 = 40.5^\circ$.

For the particular choice of input parameters, intersections at other frequencies are possible and, indeed, by finding the intersections occurring at many discrete frequencies, it is possible to generate a stability boundary. For example, in part (b) of figure 10 another solution is indicated for an attitude-rate gain of about $a_1 = 12$ with $\sigma = 1.5$ and $\omega = 0.8$. Here the $\overline{V}_2$ vector crosses the $\overline{V}_1$ vector from right to left and indicates, in accordance with the rule, that the solution is an unstable limit cycle. Thus, for amplitudes such that $\beta_0/\beta_l < 1.5$, the system is stable whereas for $\beta_0/\beta_l > 1.5$, the system is unstable.

Stability boundaries for the nonlinear response mode may, in general, be categorized in accordance with the four regions defined in figure 11. As noted, the regions are illustrated for a particular value of a_0 and are defined in terms of the attitude-rate gain a_1 and the amplitude ratio σ which is defined as the ratio of the forcing amplitude β_0 to the limit amplitude β_l (eqs. (10)). Along the $\sigma = 0$ axis, the stable region is bounded on the left

by a lower limit on a_1. For attitude-rate
gains less than this value, the system is
unstable. On the right, that portion of
the boundary falling along the $\sigma = 0$ axis
is bounded by an upper limit on a_1 above
which stable limit cycles occur. It should
be noted that this portion of the stability
boundary, that is, along $\sigma = 0$, can be
determined from a linear analysis and is
comparable to the information presented in
figure 8. In addition, an upper bound is
imposed on the region of stability by the
occurrence of unstable limit cycles. This
upper bound manifests itself in the form of
an amplitude ratio (σ) level for which the system becomes unstable if exceeded.
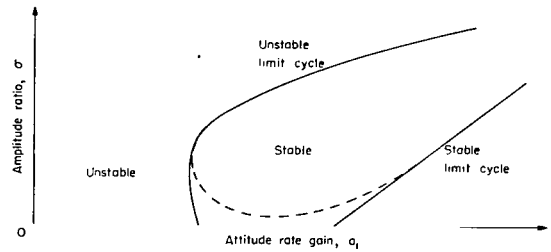For amplitude ratios less than this critical level, the system is stable.

Figure 11.- Classification of stability boundaries for
a constant a_0.

If the region of stability does not intersect the $\sigma = 0$ axis, as shown
by the dashed line in figure 11, the system response is either unstable or char-
acterized by a stable limit cycle and is indicative of a completely undesirable
set of control-system-parameter values. Control parameters should be chosen so
as to preclude the occurrence of stable limit cycles in order to insure that the
system will converge back to the equilibrium, represented by the $\sigma = 0$ axis,
when the disturbing influences terminate.

Results are presented in fig-
ure 12 for other solutions of equa-
tions (28) when other values of the
parameters under consideration are
scrutinized for possible limit cycles.
Here a damping ratio of $\xi = 0.4$ is
considered and the amplitude ratio σ
is plotted against the rate gain a_1
with the frequency ω crossplotted
as a parameter. Graphical solutions
are indicated by the solid curves for
four engine frequencies $\omega_n = 2, 3, 4,$
and 5 and for several different val-
ues of the attitude gain a_0.

(a) $a_0 = 10$.

(b) $a_0 = 20$.

Figure 12.- Nonlinear stability boundaries for $\xi = 0.4$.

Part (a) of figure 12, which
shows solutions for $\xi = 0.4$ and
$a_0 = 10$, may be interpreted as fol-
lows: Consider, for example, the
curve for $\omega_n = 2$. With $a_1 = 8$ the
amplitude ratio is about $\sigma = 2$, the
highest value considered. Analysis
in the gain-phase plane reveals this
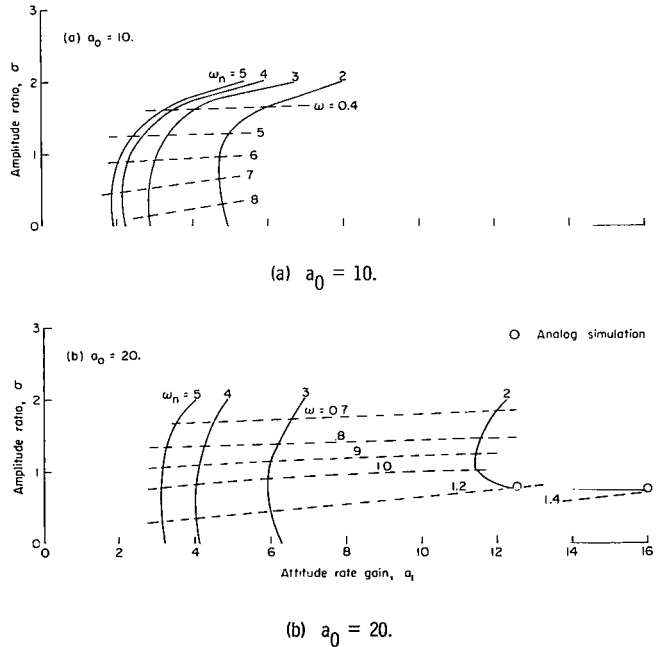point to be an unstable limit cycle.
Hence, the system is divergent for

25

$\sigma > 2$ and convergent for $\sigma < 2$. The corresponding operating frequency is about $\omega = 0.3$ radian per second. Decreasing the rate gain a_1 produces a decrease in the amplitude ratio until finally at about an $a_1 = 4.7$ and $\sigma = 0.95$, the curve drops almost vertically to $\sigma = 0$. This lower limiting value of the rate gain (on $\sigma = 0$) represents the limiting point between the stable and unstable modes of the linear system (fig. 8) for $a_0 = 10$, $\omega_n = 2$, and $\xi = 0.4$. Further decrease in the rate gain a_1 requires an increase in the engine frequency ω_n for stability of the linear system to be maintained, as was ascertained previously. Although not shown in part (a) of figure 12, it should be noted that at a higher level of the attitude-rate gain a_1, the $\omega_n = 2$ curve will break away from the $\sigma = 0$ axis as will the $\omega_n = 3$, 4, and 5 curves. (See, for example, parts (c), (d), and (e) of fig. 12.) The value of rate gain at which this breakaway occurs is equal to the upper limit value of a_1 determined from the linear analysis.

In part (b) of figure 12, the effect of increasing the attitude gain a_0 may be noted. Here the $\omega_n = 2$ curve is again multivalued with the amplitude ratio σ; and instead of approaching a discrete value of a_1 at $\sigma = 0$, it reaches a lower limiting value of about $a_1 = 11.4$ and then reverses direction, σ remaining almost constant with increasing values of a_1. Whereas the upper part of the curve denotes an unstable (divergent) limit cycle, the lower part indicates a stable (converging) limit cycle. Increasing the engine frequency to $\omega_n = 3$ produces a curve of similar shape, but which intersects the $\sigma = 0$ axis. The lower limiting value of rate gain is about $a_1 = 6.3$ which agrees well with the linear results (fig. 8). The curves for $\omega_n = 4$ and $\omega_n = 5$ also give lower limiting values for a_1 which agree well with the values obtained from the linear analysis.

Stability boundaries for $a_0 = 30$, 40, and 50 are shown in the remaining parts of figure 12. For example, part (c) of figure 12, which shows solutions for an attitude gain of $a_0 = 30$, indicates that a stable limit cycle would dominate the response for an engine frequency of $\omega_n = 2$ and attitude-rate gains a_1 greater than 20. The linear analysis indicates the system to be unstable for this combination of parameters. Hence, the response is divergent for small amplitudes, but as the amplitudes grow, the response converges to a constant-amplitude oscillation with an amplitude ratio of about $\sigma = 1$, depending on the rate gain. If the engine frequency is increased to $\omega_n = 3$, the lower limit on the rate gain is about $a_1 = 11$ (along $\sigma = 0$). For rate gains
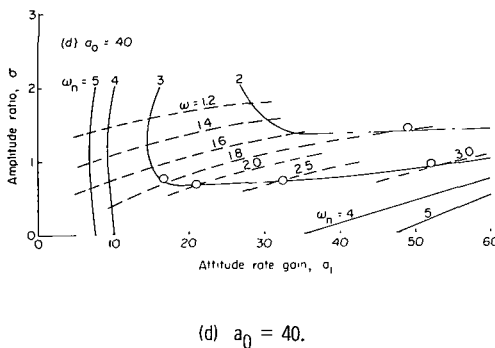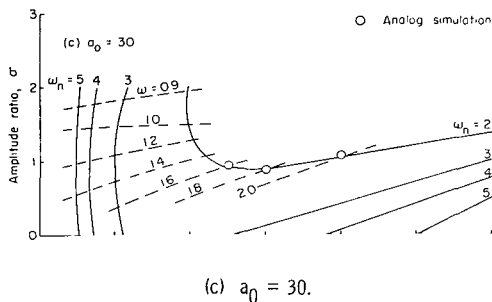

(c) $a_0 = 30$.

(d) $a_0 = 40$.

Figure 12.- Continued.

lower than about $a_1 = 11$, the system is
unstable. The upper limit for stability is
about $a_1 = 26$ and larger rate gains produce
stable limit cycles. It should be noted that
in the latter part of the region, the con-
stant ω curves (dashed lines) approached
the constant ω_n curves (solid lines) almost
tangentially. For this reason the frequency
ω is not crossplotted in this area and the
curves are faired. Increasing the engine
frequency to $\omega_n = 4$ and 5, respectively,
gives even greater latitude in the choice of
the rate gain a_1. Of course, an upper limit
is imposed on the amplitude σ which, if
exceeded, throws the time-fixed system into a

(e) $a_0 = 50$.

Figure 12.- Concluded.

diverging (unstable) mode. With attitude gains of $a_0 = 40$ and 50 as illus-
trated in parts (d) and (e), higher engine frequencies, for example $\omega_n = 4$,
are required to preclude the occurrence of stable limit cycles.

Increasing the damping ratio to $\xi = 0.7$, as summarized in figure 13, has
the effect of shifting the curves to the right so that the stable limit cycles
occur at higher values of the attitude-rate gain a_1, although it appears that
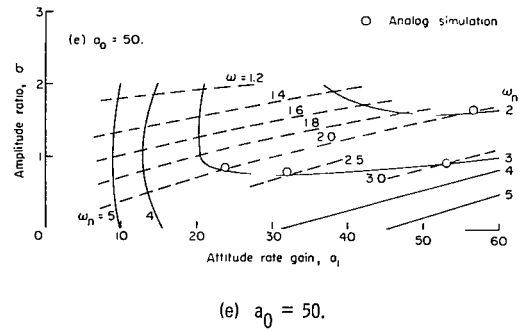
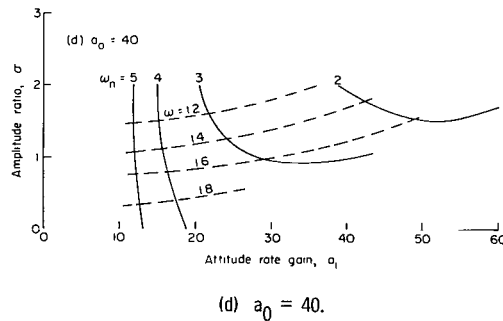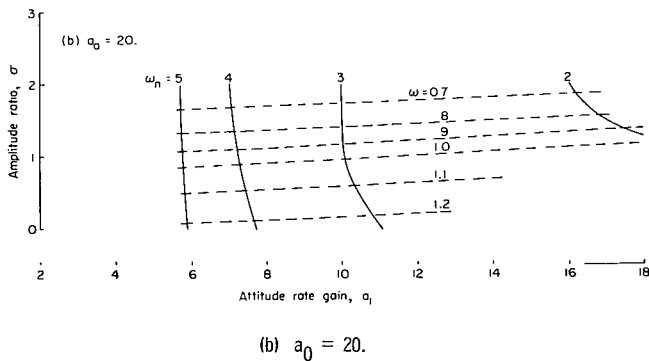(a) $a_0 = 10$.

(c) $a_0 = 30$.

(b) $a_0 = 20$.

(d) $a_0 = 40$.
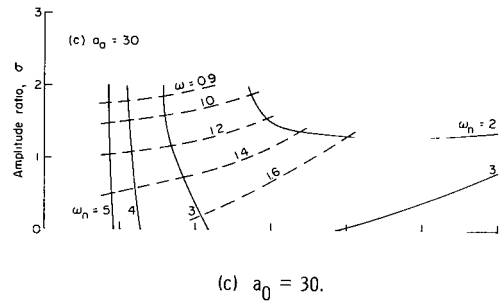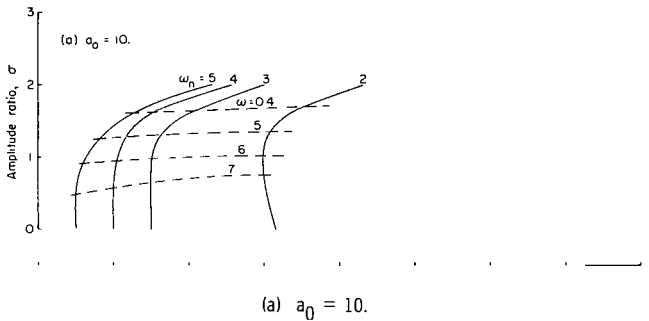
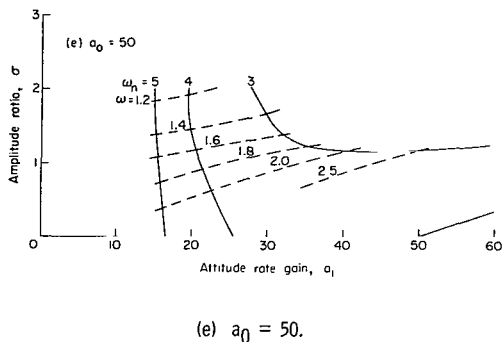Figure 13.- Nonlinear stability boundaries for $\xi = 0.7$.

(e) $a_0 = 50$.

Figure 13.- Concluded.

slightly higher engine frequencies ω_n are required for linear stability. Near the lower limiting values of the rate gain a_1, where a transition from an unstable to a stable limit cycle is possible, the gain-phase analysis is inaccurate as to whether an intersection represents a converging or diverging mode. However, increasing the rate gain in order to move away from these marginal cases produces more discernible intersections. At these higher values of a_1, an analog-computer simulation of the system provided a check on the stable limit cycles as given by the gain-phase analysis. Analog computer checkpoints are indicated by circles and are discussed briefly in the following section.

Analog-Computer Verification

An analog-computer simulation of the launch vehicle was used to check the stability bounds obtained by the describing-function analysis. Analog-computer checkpoints are shown in figure 12 by circles and indicate stable limit cycles. For example, in part (d) of figure 12, which shows the resulting stability boundaries for $a_0 = 40$ and $\xi = 0.4$, there is a checkpoint at about $a_1 = 52$ and an amplitude of about $\sigma = 0.95$. This point is associated with an engine frequency of $\omega_n = 3$ and indicates a cyclic frequency for the limit cycle of about $\omega = 3$ radians per second. As is apparent from the figure, the agreement is very good. Decreasing the rate gain, there are several additional checkpoints at frequencies of $\omega = 2.5$, 2.0, and 1.8 radians per second for an engine frequency of $\omega_n = 3$ and the agreement is again good. Further decrease in the rate gain a_1 did not yield as good agreement since these points fall closer to the condition of marginal stability. In addition, it was not possible to check the upper branch of these curves, which represents unstable limit cycles, because the effective damping is very low along this part of the boundary.

CONCLUDING REMARKS

A stability analysis has been conducted on a launch vehicle having a type of nonlinear thrust vectoring. The frequency-response characteristics of nonlinearities, which arise from control forces produced by an amplitude-limited engine rotating through large gimbal angles, were approximated by a describing function. By representing the linear portion of the closed-loop system by gain-phase plots, stability bounds were determined graphically for a range of parameter values. Selected stable limit cycles, predicted by the describing function analysis, were verified by simulating some of these sustained, constant-amplitude oscillations on an analog computer. The frequency and amplitude of these stable limit cycles were in good agreement with the values

measured from the analog time histories. The small amplitude results were checked by linearizing the equations and doing an independent root-locus analysis. An interesting aspect of the study was that the describing function for the nonlinearities investigated exhibited a type of jump behavior.

Langley Research Center,
    National Aeronautics and Space Administration,
        Langley Station, Hampton, Va., June 22, 1965.

APPENDIX A

SINUSOIDAL RESPONSE OF CONTROL ENGINE

This appendix is devoted to determining the sinusoidal response character-
istics of an amplitude-limited-control engine. The response equations are
derived for both the linear and nonlinear modes.

Analysis

For the analysis presented herein, the characteristics of the control
engine dynamics are given by the second-order constant-coefficient linear dif-
ferential equation

$$\ddot{\beta} + 2\xi\omega_n\dot{\beta} + \omega_n^2\beta = \omega_n^2\beta_o \sin \omega t \tag{A1}$$

subject to an amplitude constraint (boundary condition) as defined by the fol-
lowing two equations:

$$|\beta| \leqq \beta_l \tag{A2}$$

$$\dot{\beta} = 0 \qquad \left(\beta = \pm\beta_l\right) \tag{A3}$$

Equation (A1) can be interpreted as describing the dynamical state of a
linear spring-mass oscillator with an attached viscous dashpot (damper) when
excited by a sinusoidal forcing function with amplitude β_o and circular fre-
quency ω. The parameter ω_n may therefore be thought of as the undamped
natural frequency of the system, ξ the viscous damping ratio, and β_l the
limit amplitude. For certain combinations of the input parameters, that is,
ω/ω_n, ξ, and β_o/β_l, the unlimited linear response may exceed a particular
value of β_l under consideration. Solution of equation (A1) requires, under
these circumstances, a joint consideration of the boundary conditions
(eqs. (A2) and (A3)) and the resulting response of the system is nonlinear.
If, however, $|\beta| \leqq \beta_l$, the system behaves linearly.

In a physically realizable system a dissipative mechanism (buffer) would
be employed with the amplitude limits. The effect of any such buffer arrange-
ment has been neglected herein with the assumption that the velocity $\dot{\beta}$ is
instantaneously reduced to zero when limiting occurs (when $\beta = \pm\beta_l$). As will
be apparent later, this assumption produces an output waveform which is piece-
wise continuous for the nonlinear response mode.

The simultaneous solution of equations (A1), (A2), and (A3) yields the
desired response for any combinations of the damping ratio ξ, frequency ratio

ω/ω_n, and amplitude ratio β_o/β_l. The solution may be generalized by substituting the following nondimensional parameters:

$$\left. \begin{array}{c} \tau = \left(\dfrac{\omega}{2\pi}\right)t \\[12pt] \Omega = \dfrac{\omega}{\omega_n} \\[12pt] \Omega_d = \dfrac{\omega}{\omega_d} = \dfrac{\Omega}{\sqrt{1 - \xi^2}} \\[12pt] \sigma = \dfrac{\beta_o}{\beta_l} \\[12pt] \delta = \dfrac{\beta}{\beta_o} \end{array} \right\} \qquad (A4)$$

Differentiating $\beta = \beta_o\delta$ and using $\tau = \left(\dfrac{\omega}{2\pi}\right)t$ produces

$$\frac{d\beta}{dt} = \beta_o \frac{d\delta}{d\tau} \frac{d\tau}{dt} = \frac{\beta_o\omega}{2\pi} \frac{d\delta}{d\tau} \qquad (A5a)$$

and a second differentiation produces, in a similar manner, the following:

$$\frac{d^2\beta}{dt^2} = \beta_o\left(\frac{\omega}{2\pi}\right)^2 \frac{d^2\delta}{d\tau^2} \qquad (A5b)$$

Equations (A1), (A2), and (A3) may therefore be rewritten in a nondimensional form by using the results of equations (A4) and (A5).

$$\frac{d^2\delta}{d\tau^2} + 2\xi\left(\frac{2\pi}{\Omega}\right)\frac{d\delta}{d\tau} + \left(\frac{2\pi}{\Omega}\right)^2\delta = \left(\frac{2\pi}{\Omega}\right)^2 \sin 2\pi\tau \qquad (A6)$$

$$|\delta| \leqq \frac{1}{\sigma} \qquad (A7)$$

$$\frac{d\delta}{d\tau} = 0 \qquad\qquad \left(\delta = \pm \frac{1}{\sigma}\right) \qquad (A8)$$

Unless stated otherwise, equations (A6), (A7), and (A8) will hereafter be referred to as "the system" where it is assumed that nondimensionality is implied.

The solution of the system equations may be conveniently divided into two parts governing the linear and nonlinear modes of operations. The linear response is determined first. If $\delta \leqq \frac{1}{\sigma} \left(\beta \leqq \beta_l \right)$, the constraint equations (A7) and (A8) do not influence the solution. Hence, equation (A6) may be solved by using the methods of linear ordinary differential equations or operational techniques (Laplace transforms) and is given by the following equations:

$$\delta(\tau) = A \sin\left(2\pi\tau - \phi_2\right) \qquad \left(\delta \leq \frac{1}{\sigma}\right) \qquad \text{(A9)}$$

where

$$A = \frac{1}{\sqrt{4\xi^2\Omega^2 + \left(1 - \Omega^2\right)^2}} \qquad \text{(A10)}$$

$$\phi_2 = \tan^{-1}\left(\frac{2\xi\Omega}{1 - \Omega^2}\right) \qquad \text{(A11)}$$

Equation (A9) is the steady-state linear response of the system when excited with a sinusoidal forcing function and is applicable only so long as $A \leqq 1/\sigma$.

It will now be shown that the nonlinear case $(A > 1/\sigma)$ can be constructed as a piecewise continuous function. Figure 14 illustrates a typical output waveform when the system is operating in the nonlinear mode. The derivation begins by noting that as soon as the system leaves the limit at $\tau = \tau_2$ and $\tau = \tau_4$, it is once again linear. Thus, this portion of the solution can be obtained by the methods of linear analysis.

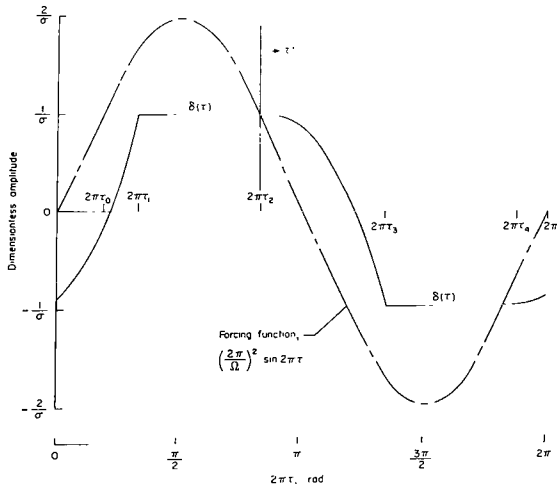Figure 14.- Typical steady-state output waveform of the amplitude-limited control engine.

Consider a shifted time reference noted as τ' (where $\tau' = \tau - \tau_2$) in figure 14. At $\tau' = 0$, the state of the system by virtue of the amplitude constraint is given as follows:

$$\left.\begin{array}{l} \delta = \dfrac{1}{\sigma} \\[2ex] \dfrac{d\delta}{d\tau} = 0 \end{array}\right\} \qquad \text{(A12)}$$

As the system leaves the limit at $\tau' = 0$, the fall-off response can be determined by solving the differential equation

$$\frac{d^2\delta}{d\tau'^2} + 2\xi\left(\frac{2\pi}{\Omega}\right)\frac{d\delta}{d\tau'} + \left(\frac{2\pi}{\Omega}\right)^2 \delta = \left(\frac{2\pi}{\Omega}\right)^2 \sin\left[2\pi\left(\tau' + \tau_2\right)\right] \tag{A13}$$

subject to the initial conditions expressed by equations (A12). The general solution may be formulated by the straightforward methods of linear analysis and is stated as follows:

$$\delta(\tau') = A \sin\left(2\pi\tau' + \phi_1\right) + Be^{\frac{-2\pi\xi\tau'}{\Omega}} \sin\left(\frac{2\pi}{\Omega_d} \tau' + \phi_0\right) \tag{A14}$$

where A and ϕ_2 are given by equations (A10) and (A11) and the remaining parameters are defined as follows:

$$\left.\begin{array}{l} B = \dfrac{\dfrac{1}{\sigma} - A \sin \phi_1}{\sin \phi_0} \\[20pt] \Omega_d = \dfrac{\Omega}{\sqrt{1 - \xi^2}} \\[20pt] \phi_0 = \tan^{-1}\left[\dfrac{\dfrac{1}{\sigma} - A \sin \phi_1}{\xi \dfrac{\Omega_d}{\Omega}\left(\dfrac{1}{\sigma} - A \sin \phi_1\right) - \Omega_d A \cos \phi_1}\right] \\[20pt] \phi_1 = 2\pi\tau_2 - \phi_2 \end{array}\right\} \tag{A15}$$

If it is assumed for the present that τ_2 and τ_4 are known, the output waveform of the system for the situation involving limiting can be established as a piecewise continuous function. For $0 \leqq \tau \leqq \tau_1$, the initial condition must be changed from $\frac{1}{\sigma}$ to $-\frac{1}{\sigma}$ and the argument in equation (A14) must be replaced by $2\pi\tau' = 2\pi\tau + \left(\pi - 2\pi\tau_2\right)$ as is apparent from figure 14. Therefore,

$$\delta(\tau) = -A \sin\left(2\pi\tau + \pi - \phi_2\right) - B\left\{\exp\left[-\frac{2\pi\xi}{\Omega}\left(\tau - \tau_2 + \frac{1}{2}\right)\right]\right\} \sin\left[\frac{2\pi}{\Omega_d}\left(\tau - \tau_2 + \frac{1}{2}\right) + \phi_0\right]$$

$$\left(0 \leqq \tau \leqq \tau_1\right) \tag{A16}$$

33

During the next time interval, the system is on the positive limit so that

$$\delta(\tau) = \frac{1}{\sigma} \qquad \left(\tau_1 \leqq \tau \leqq \tau_2\right) \qquad \text{(A17)}$$

The response during the next interval of time can be obtained by substituting $2\pi\tau' = 2\pi\tau - 2\pi\tau_2$ into equation (A14):

$$\delta(\tau) = A \sin\left(2\pi\tau - \phi_2\right) + B\left\{\exp\left[-\frac{2\pi\xi}{\Omega}(\tau - \tau_2)\right]\right\} \sin\left[\frac{2\pi}{\Omega_d}(\tau - \tau_2) + \phi_0\right]$$

$$\left(\tau_2 \leqq \tau \leqq \tau_3\right) \qquad \text{(A18)}$$

In a similar manner,

$$\delta(\tau) = -\frac{1}{\sigma} \qquad \left(\tau_3 \leqq \tau \leqq \tau_4\right) \qquad \text{(A19)}$$

Finally, for the last interval the sign on the initial condition must again be changed to $-\frac{1}{\sigma}$ and the argument in equation (A14) must be replaced by $2\pi\tau' = 2\pi\tau - 2\pi\tau_4$

$$\delta(\tau) = -A \sin\left(2\pi\tau - \pi - \phi_2\right) - B\left\{\exp\left[-\frac{2\pi\xi}{\Omega}(\tau - \tau_4)\right]\right\} \sin\left[\frac{2\pi}{\Omega_d}(\tau - \tau_4) + \phi_0\right]$$

$$\left(\tau_4 \leqq \tau \leqq 1.0\right) \qquad \text{(A20)}$$

where from figure 14

$$\tau_3 = \tau_1 + \frac{1}{2} \qquad \text{(A21)}$$

$$\tau_4 = \tau_2 + \frac{1}{2} \qquad \text{(A22)}$$

The times τ_2 and τ_3 may now be determined. From equation (A6) it is apparent that $\left(\frac{2\pi}{\Omega}\right)^2 \sin 2\pi\tau$ represents a disturbing force (in nondimensional notation) applied to the system whereas $\left(\frac{2\pi}{\Omega}\right)^2 \delta$ may be interpreted as a non-dimensional elastic restoration or spring force. During limiting, the spring force equals $\left(\frac{2\pi}{\Omega}\right)^2\!\Big/\sigma$. If $\sigma > 1.0$, that is, $\beta_0 > \beta_l$, the disturbing force is greater than the spring force and the system will remain on the limit until the

disturbing force equals the spring force. Equating the spring force (fig. 14) to the disturbing forces produces an equation for time τ_0.

$$\tau_0 = \frac{1}{2\pi} \sin^{-1}\left(\frac{1}{\sigma}\right) \qquad (\sigma > 1.0) \qquad (A23)$$

Since the input is a periodic function, the time at which the system departs from the positive limit is given by the following equation:

$$\tau_2 = \frac{1}{2} - \tau_0 \qquad (A24)$$

If τ_2 is known, it is possible to return to equation (A18) and solve for τ_3 since

$$\delta(\tau) = A \sin\left(2\pi\tau_3 - \phi_2\right) + B\left\{\exp\left[-\frac{2\pi\xi}{\Omega}\left(\tau_3 - \tau_2\right)\right]\right\} \sin\left[\frac{2\pi}{\Omega_d}\left(\tau_3 - \tau_2\right) + \phi_0\right] = -\frac{1}{\sigma}$$

$$(A25)$$

If, however, $\sigma \lessgtr 1.0$ $\left(\beta_0 \lessgtr \beta_l\right)$, the disturbing force is always less than or equal to the maximum spring force $\left(\frac{2\pi}{\Omega}\right)^2 / \sigma$. It should be noted that for this situation it is still possible for the system to limit because of the overshoot associated with low damping and/or a near-resonance frequency ratio. A cusped response is obtained in this case as illustrated in figure 4(c). Under this condition, periodicity requires that

$$\tau_3 - \tau_2 = \frac{1}{2} \qquad (A26)$$

and by using equations (A25) and (A26), both τ_2 and τ_3 can be determined.

The analytical solution was checked by simulating the original constant-coefficient differential equations (eqs. (A6) to (A8)) on an analog computer. The results are presented in figure 4 for several combinations of the input parameters. As is apparent from the figures, the comparison is very good. The sinusoidal response equations for both the linear and nonlinear modes are summarized in the section "Derivation of the Describing Function."

APPENDIX B

NUMERICAL DATA FOR THE MAXIMUM DYNAMIC PRESSURE CONDITION

The following numerical values were used for the coefficients required in equations (1) and (2):

$$\frac{\rho V}{m} \int_0^l S'(x)dx = -8.955(10)^{-3}$$

$$\frac{T_b - D}{m} - \frac{\rho V^2}{m} \int_0^l S'(x)dx = 1.036(10)^3$$

$$\frac{\rho V}{m} \int_0^l (x - \bar{x}) S'(x)dx = -6.92$$

$$\frac{T_c}{m} = 42.7$$

$$\frac{\rho V}{I} \int_0^l (x - \bar{x}) S'(x)dx = -9.764(10)^{-6}$$

$$\frac{\rho V^2}{I} \int_0^l (x - \bar{x}) S'(x)dx = -0.1992$$

$$\frac{\rho V}{I} \int_0^l (x - \bar{x})^2 S'(x)dx = -2.655(10)^{-2}$$

$$\frac{T_c \bar{x}}{I} = 7.29(10)^{-2}$$

REFERENCES

1. Kochenburger, Ralph J.: A Frequency Response Method for Analyzing and Syn-
      thesizing Contractor Servomechanisms. Trans. AIEE, vol. 69, pt. I, 1950,
      pp. 270-284.

2. Truxal, John G.: Automatic Feedback Control System Synthesis. McGraw-Hill
      Book Co., Inc., 1955.

3. Graham, Dunstan; and McRuer, Duane: Analysis of Nonlinear Control Systems.
      John Wiley & Sons, Inc., c.1961.

4. Lineberry, Edgar C., Jr.; and Foudriat, Edwin C.: Application of Describing-
      Function Analysis to the Study of an On-Off Reaction-Control System. NASA
      TN D-654, 1961.

5. Backus, F. I.: Describing Functions for Nonlinear Electrohydraulic Gimbaled
      Rocket-Engine Position Servos With Application to Closed-Loop Control
      Systems. Rept. No. AE60-0287 (Contract No. AF 04(647)-299), Convair-
      Astronautics, June 10, 1960.

6. Kachigan, K.: The General Theory and Analysis of a Flexible Bodied Missile
      With Autopilot Control. Rept. ZU-7-048 (Contract No. AF04(645)-4),
      CONVAIR, Nov. 11, 1955.

7. Miles, J. W.; and Young, Dana: Generalized Missile Dynamics Analysis.
      III - Aerodynamics. GM-TR-0165-00360, Space Technol. Lab., The Ramo-
      Wooldridge Corp., Apr. 7, 1958.

"The aeronautical and space activities of the United States shall be conducted so as to contribute . . . to the expansion of human knowledge of phenomena in the atmosphere and space. The Administration shall provide for the widest practicable and appropriate dissemination of information concerning its activities and the results thereof."

—NATIONAL AERONAUTICS AND SPACE ACT OF 1958

NASA SCIENTIFIC AND TECHNICAL PUBLICATIONS

TECHNICAL REPORTS: Scientific and technical information considered important, complete, and a lasting contribution to existing knowledge.

TECHNICAL NOTES: Information less broad in scope but nevertheless of importance as a contribution to existing knowledge.

TECHNICAL MEMORANDUMS: Information receiving limited distribution because of preliminary data, security classification, or other reasons.

CONTRACTOR REPORTS: Technical information generated in connection with a NASA contract or grant and released under NASA auspices.

TECHNICAL TRANSLATIONS: Information published in a foreign language considered to merit NASA distribution in English.

TECHNICAL REPRINTS: Information derived from NASA activities and initially published in the form of journal articles.

SPECIAL PUBLICATIONS: Information derived from or of value to NASA activities but not necessarily reporting the results of individual NASA-programmed scientific efforts. Publications include conference proceedings, monographs, data compilations, handbooks, sourcebooks, and special bibliographies.

Details on the availability of these publications may be obtained from:

SCIENTIFIC AND TECHNICAL INFORMATION DIVISION

NATIONAL AERONAUTICS AND SPACE ADMINISTRATION

Washington, D.C. 20546